Key Engineering Materials
ISSN: 1662-9795, Vol. 1047, pp 83-93

Submitted: 2025-12-19
Accepted: 2026-02-11
Online: 2026-04-13

Investigation of WAAM-PAW Fabricated 316L Steel/Invar 36 Nb Alloys for the Development of Functionally Graded Materials

Weber Lucas[1,2,a*], Hor Anis[1,b], Ratsifandrihana Léon[2,c] and Alcaraz Mathilde[2,d]

[1]Clément Ader Institute, Toulouse University, CNRS, ISAE-SUPAERO, France

[2]Segula Technologies, France

[a*]Lucas.WEBER@isae-supaero.fr, [b]Anis.HOR@isae-supaero.fr,
[c]Leon.RATSIFANDRIHANA@segula.fr, [d]Mathilde.ALCARAZ@segula.fr

Keywords: wire arc additive manufacturing (WAAM), plasma arc welding (PAW), functionally graded materials (FGM), 316L stainless steel, invar 36 Nb, microhardness, mechanical properties, thermal expansion coefficient (CTE), corrosion resistance.

Abstract. Functionally graded materials represent a promising strategy for locally optimizing component properties while reducing both economic and environmental costs. To date, no study has addressed the development of a compositional gradient between 316L stainless steel and Invar 36 using the Wire Arc Additive Manufacturing (WAAM) process, despite the strong potential of this material combination. Indeed, such a gradient would combine the very low coefficient of thermal expansion (CTE) of Invar 36 with the low cost and excellent chemical resistance of 316L stainless steel. A particularly relevant application for this type of gradient is the storage of hydrogen or liquefied natural gas, where tanks are subjected to severe thermal stresses due to cryogenic operating temperatures. In addition, these structures must withstand aggressive environments and hydrogen exposure, which can induce material embrittlement, while maintaining sufficient mechanical properties to ensure structural integrity during service. Designing an optimal gradient therefore requires a detailed understanding of how mechanical, thermal, and chemical properties evolve with chemical composition. This study provides a preliminary assessment of these evolutions. The results show that the addition of 15–25 wt.% Invar 36 to 316L leads to a reduction in microhardness and ultimate tensile strength (UTS), associated with the disappearance of ferritic and σ phases, while significantly enhancing ductility. At higher Invar 36 contents, microhardness increases and ductility decreases due to carbide formation. From a thermal standpoint, the CTE does not follow a linear trend: it remains high up to approximately 75 wt.% Invar 36 Nb, then decreases sharply as the ferromagnetic behavior characteristic of Invar becomes dominant. Corrosion resistance remains satisfactory for Invar 36 contents below 15 wt.%, whereas higher contents lead to reduced chemical performance due to chromium dilution. Overall, these findings establish clear criteria for selecting optimal compositions in the design of a 316L–Invar 36 compositional gradient. They provide an essential foundation for the development, via WAAM, of robust and high-performance functionally graded materials suitable for applications requiring high dimensional stability, good chemical resistance, and controlled costs.

1. Introduction

Technological development requires materials capable of withstanding multiple stresses (mechanical, chemical, thermal, etc.) that are becoming increasingly severe. High-performance metals, such as nickel-based or titanium alloys, meet these needs but remain costly and have a high environmental impact. One alternative is to design multi-material structures in which different conventional alloys are locally assembled to achieve optimal properties in specific areas. However, the interfaces between these materials are critical areas that can lead to premature failure, particularly in cases where there are sudden changes in microstructure or properties (i.e. thermal expansion coefficient) [1]. Additive manufacturing processes offer a solution by allowing the introduction of composition gradients and thus gradual transitions in properties [2]. Among these, the WAAM process stands out as one of the most promising for easily producing large gradient parts [3].

Different functional gradient materials (FGMs) have already been studied, particularly by combining stainless steels with Inconels to combine the high performance of these superalloys with the low cost of stainless steels. Rodrigues et al. manufactured an FGM using WAAM with 316L steel and Inconel 625 [4]. However, the appearance of brittle phases degraded the mechanical properties [4]. FGMs involving titanium alloys have also been explored for the same reasons. Chen et al. combined Ti-6Al-4V with 316L stainless steel [5]. This time, cracks appeared at the interface. It is therefore essential to develop and characterize intermediate alloys to design viable gradients. This includes optimizing manufacturing parameters and choosing chemical compositions to limit defects and the formation of undesirable phases.

Furthermore, FGMs using Invar 36 have been little studied, even though this material has a very low coefficient of thermal expansion up to its Curie temperature (~250 °C), making it indispensable for cryogenic applications (liquid natural gas transport [6], transport of liquid hydrogen [7]) or applications requiring high dimensional stability (i.e. molds for polymers or composites [8], bonding composite panels on spacecraft [9] and tooling [10]). However, its high cost and poor chemical performance (i.e. corrosion and hydrogen resistance) justify its combination with stainless steel. Hofmann et al. manufactured an FGM by Laser Metal Deposition (LMD) by combining Invar 36 and 304L steel to reduce thermal expansion without loss of mechanical properties [9]. Arbogast et al. observed a 42% reduction in surface expansion after WAAM deposition of Invar 36 on steel [10]. Using the LPBF process, Guo et al. demonstrated that an appropriate choice of composition gradient between Invar 36 and 316L steel allows the properties to be controlled [11]. However, no study has yet investigated the development of an FGM combining stainless steel and Invar 36 using the WAAM process. This work, therefore, proposes to study different alloys resulting from the combination of 316L stainless steel and Invar 36 using a WAAM-Plasma process. The mechanical, thermal, and chemical properties of these alloys are evaluated to identify the most suitable compositions for obtaining an optimized FGM according to the application.

2. Materials and Methods

The materials used are supplied in the form of 1.2 mm diameter wire spools. Two alloys are used: Invar 36 Nb and 316L austenitic stainless steel. Table 1 shows their chemical composition. Invar 36 is deliberately doped with niobium and carbon to reduce the risk of solidification cracking, which is common when welding conventional Invar 36. Osuki et al. showed that sensitivity to these cracks decreases significantly when the composition contains approximately 0.2% C and 1.5% Nb [12]. In this study, several intermediate alloys were developed. These intermediate compositions were obtained by adjusting the feed rate of the two wires during the deposition process.

Table 1. Chemical composition in weight percent (wt.%) of the two alloys studied.

		Fe	Cr	Ni	Mo	Mn	Si	C	Nb	Ti
316L		Balance	18.5	12.0	2.80	1.70	0.80	0.02	/	/
Invar 36 Nb		Balance	/	36	/	0.40	0.15	0.20	1.30	0.20

The deposition process used is illustrated in Figure 1. It is the WAAM-PAW (Plasma Arc Welding) process. At the center of the torch, there is a tungsten electrode, around which a plasma gas is injected. An electric arc is then established between the torch and the substrate, generating a very high-temperature plasma. This plasma allows the two filler filaments to melt and form the molten pool. A shielding gas, argon, is used to protect the molten pool from the ambient atmosphere. The torch and filler wires move along a programmed trajectory, allowing the part to be manufactured by successive deposition of beads. The entire process is carried out in an inert argon atmosphere to minimize oxidation, which occurs despite the presence of the shielding gas around the molten pool. Using this process, single-bead walls measuring 140 × 6 × 100 mm were manufactured for the various alloys studied, using the deposition parameters shown in Table 2.

Table 2. Manufacturing parameters.

Parameter	Value
Total wire feeding speed [mm/sec]	40
Torch speed [mm/sec]	5
Dwell time [sec]	45
Plasma gas flow rate [L/min]	1,5
Shielding gas flow rate [L/min]	15
Oxygen [ppm]	200 – 800
Intensity [A]	230 – 155

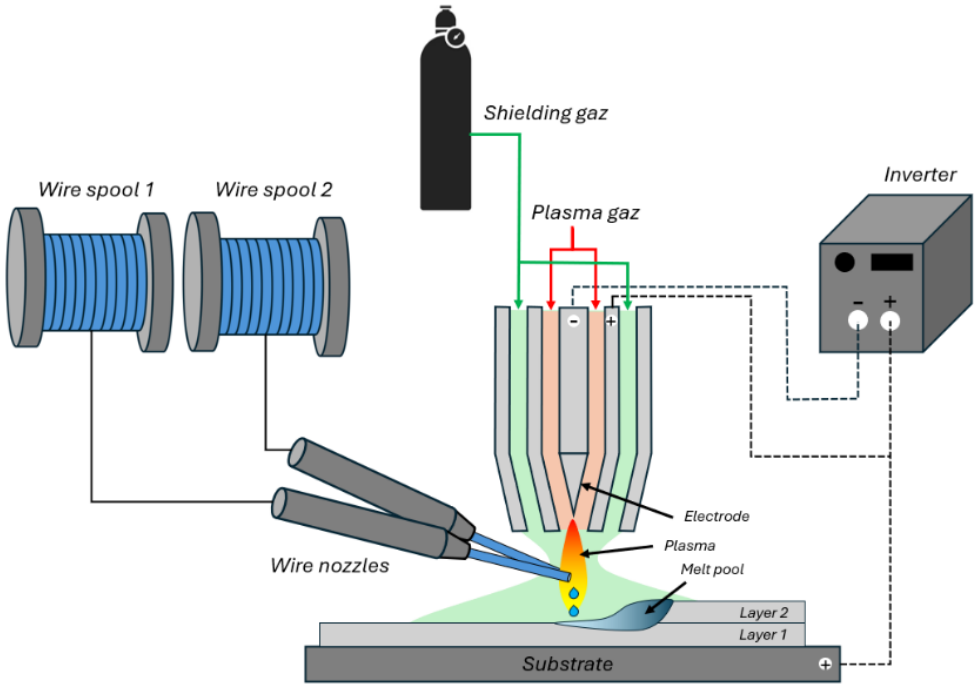

Fig. 1. Diagram of the WAAM-PAW process.

Microhardness measurements (HV5) are performed using an Innovatest Falcon 500G2 machine. A matrix of nine indents is made on a cube taken from the center of the walls. Tensile tests are performed at room temperature using a 50 kN INSTRON 5969 machine. The tensile test specimens are flat. They were taken vertically from the walls according to the geometry shown in Figure 2.

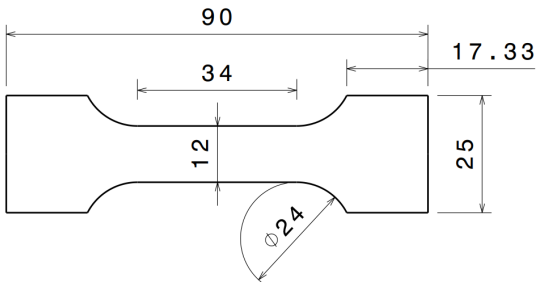

Fig. 2. Geometry of tensile test specimens (thickness = 3 mm).

Thermal expansion measurements are performed using a Netzsch TMA 402 F1/F3 Hyperion device. These tests are carried out between 25°C and 400°C with a ramp rate of 5K/min. The samples are cylinders of 6 mm in diameter and 10 mm in height. Potentiodynamic polarization tests are performed using an Origlaflex OGF+01A bench. The reference electrode is saturated calomel, the counter electrode has a platinum head, and a sample holder with a sample of the material under study constitutes the working electrode. The samples are 3 mm thick and 7,9 mm in diameter. The electrolyte solution is NaCl with a concentration of 3,5% by mass, or 0,6 mol/L. During the tests, the

free potential is recorded for 180 min. The measurement frequency is 1 Hz. The potentiodynamic polarization test is then performed over the range -300 mV to +1200 mV relative to the free potential. The scan rate is 0,1666 mV/sec.

3. Results and Discussion

Alloy Fabrication

Manufacturing parameters directly influence the development of defects, which in turn can significantly degrade the properties of the material. As shown by Jafari et al., different types of defects can develop with the WAAM process: porosity, cracks, distortions, and humping [13]. It is therefore essential to identify the optimal parameters to limit these defects, especially since these parameters may depend on the chemical composition of the deposit. Manufacturing is mainly governed by three parameters: torch speed, wire feeding speed, and welding intensity. These parameters must be carefully adjusted. Insufficient heat input can cause lacks of fusion and insufficient metallurgical bonding. Conversely, too much heat input can cause the bead to collapse and increase residual stresses. However, the total wire feeding speed must remain constant because it determines the chemical composition of the alloys produced (Table 3). Similarly, the torch speed is kept constant to ensure that the same amount of material is deposited per bead. Thus, the intensity is the only parameter adjusted to optimize manufacturability and reduce the occurrence of defects.

Table 3. Wire feeding speed for different alloys.

Chemical composition	316L wire feeding speed [mm/sec]	Invar wire feeding speed [mm/sec]
316L	40	0
75% 316L - 25% Inv36	30	10
50% 316L - 50% Inv36	20	20
25% 316L - 75% Inv36	10	30
Invar 36 Nb	0	40

The parametric optimization indicates that the optimal intensity depends directly on the wire feeding speed. Thus, 316L steel and Invar 36 Nb, both deposited at 40 mm/s, have similar optimal intensities. The parameters are therefore not adjusted according to chemical compositions, but rather according to wire feeding speeds. For the first layer, the optimal intensities are 230 A for 316L and Invar 36 Nb, and 220 A for the alloy composed of 50% 316L steel and 50% Invar 36 Nb. However, a gradual reduction in intensity is necessary to prevent the weld beads from collapsing. When the heat input has stabilized, the intensities are 180 A for 316L and Invar 36 Nb, and 155 A for the alloy with 50% 316L steel and 50% Invar 36 Nb (Table 4). In the case of 316L and Invar 36 Nb, a single wire at 40 mm/s is used. A high intensity is necessary to ensure complete melting. If the intensity is too low, the wire passes through the plasma without melting. For the alloy composed of 50% of each material, two wires, each with a feeding speed of 20 mm/s, are exposed to the plasma for a longer period of time. They therefore require a lower intensity.

Table 4. Stabilized intensity for different alloys.

Alloy	316L	90% 316L 10% Invar	80% 316L 20% Invar	70% 316L 30% Invar	60% 316L 40% Invar	50% 316L 50% Invar	Invar 36
Intensity [A]	180	175	170	165	160	155	180

When alloys require very different wire feeding speeds, a dripping phenomenon may occur. This is because the intensity has been optimized for the wire with the highest feeding speed. However, the wire with a lower feeding speed requires a lower intensity: if the intensity is too high for it, it melts periodically before reaching the molten pool, causing successive drops to form. To eliminate this phenomenon, the distance between the torch and the bead must be reduced so that the wire comes into direct contact with the previously deposited layer. In this configuration, the wire melts through radiation and conduction, and the surface tension is stabilized at the tip of the wire. It prevents the

formation of droplets. The chemical composition of the alloys obtained is then verified by EDS analyses, presented in Figure 3, and compared with the theoretical compositions. The trends observed are similar, indicating good chemical homogeneity of the deposits despite differences in wire feeding speed. The Marangoni effects and the successive remelting ensure effective mixing between 316L steel and Invar 36 Nb.

In summary, the different alloys are produced by modifying the wire feeding speeds to obtain the correct chemical composition and by adjusting the intensity to prevent the formation of defects. It is also necessary to optimize the process to prevent a drip effect and achieve a homogeneous chemical composition.

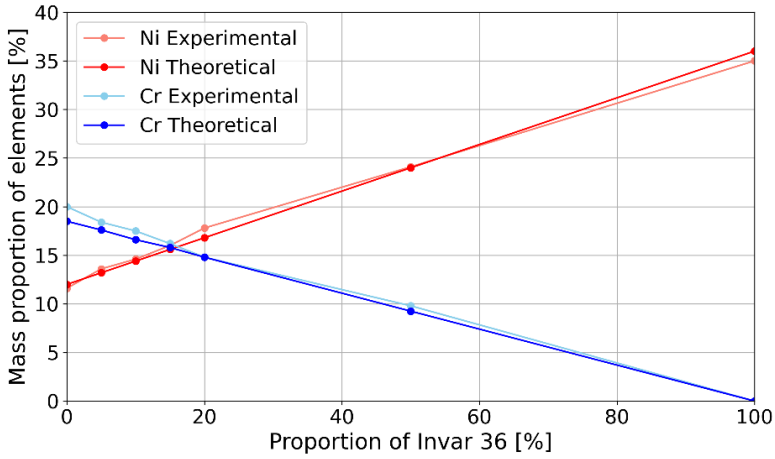

Fig. 3. Change in the mass proportion of nickel and chromium as a function of the proportion of Invar 36 Nb.

Hardness Evolution

To design an optimal gradient between 316L steel and Invar 36 Nb, it is essential to carefully select the intermediate compositions. Indeed, certain contents may have undesirable properties and should be avoided. Furthermore, the evolution of properties is not necessarily linear: if the objective is to obtain a gradual and regular variation in performance, then suitable compositions must be chosen. An initial approach to identifying these optimal compositions is to determine the alloys with the best mechanical properties and those with the worst mechanical properties. To this end, Figure 4 shows the evolution of microhardness as a function of chemical composition and correlates it to microstructures.

The hardness measured for 316L stainless steel is 165,8 HV. This value is close to that obtained by Yu et al. with a WAAM-PAW process (165–170 HV) [14], but remains lower than that obtained by other additive manufacturing processes such as WAAM-GMAW [15] or LPBF [11]. This relatively low hardness can be explained by the granular microstructure consisting of large columnar grains. When 15% Invar 36 Nb is added, the hardness drops significantly from 165,8 HV to 124,1 HV, a relative reduction of about 25%. This decrease is explained by the disappearance of the ferrite and σ phases. In the initial 316L steel, the microstructure consists of austenite, ferrite, and the σ phase, the latter being very hard but brittle. With 5% Invar 36 Nb, the σ phase remains present, but in small quantities. At 10%, the threshold beyond which the formation of ferrite and σ becomes marginal is approached: only a few fractured islands remain. With 15%, ferrite and the σ phase disappear, which explains the decrease in hardness.

Above 15% of Invar 36 Nb, hardness increases gradually with Invar content. This rise is directly related to the increasing formation of carbides in the alloy. The presence of significant proportions of niobium and carbon promotes the formation of niobium carbides, to which are added, in smaller quantities, titanium and molybdenum carbides. These carbides, which are hard phases, reinforce the material by blocking the movement of dislocations, resulting in increased hardness. Pure Invar 36 Nb has a hardness of 147,8 HV, which is lower than the values reported by Iturrioz et al. with WAAM-

CMT (174 HV) [16] or by Veiga et al. with WAAM-PAW [17]. This difference may be due to different process parameters or to the location where the hardness tests are performed, as hardness varies within the same wall. Moreover, the trend observed in this study differs significantly from that reported by Guo et al. [11] or Hofmann et al. [9], as the chemical composition of the Invar used here is different.

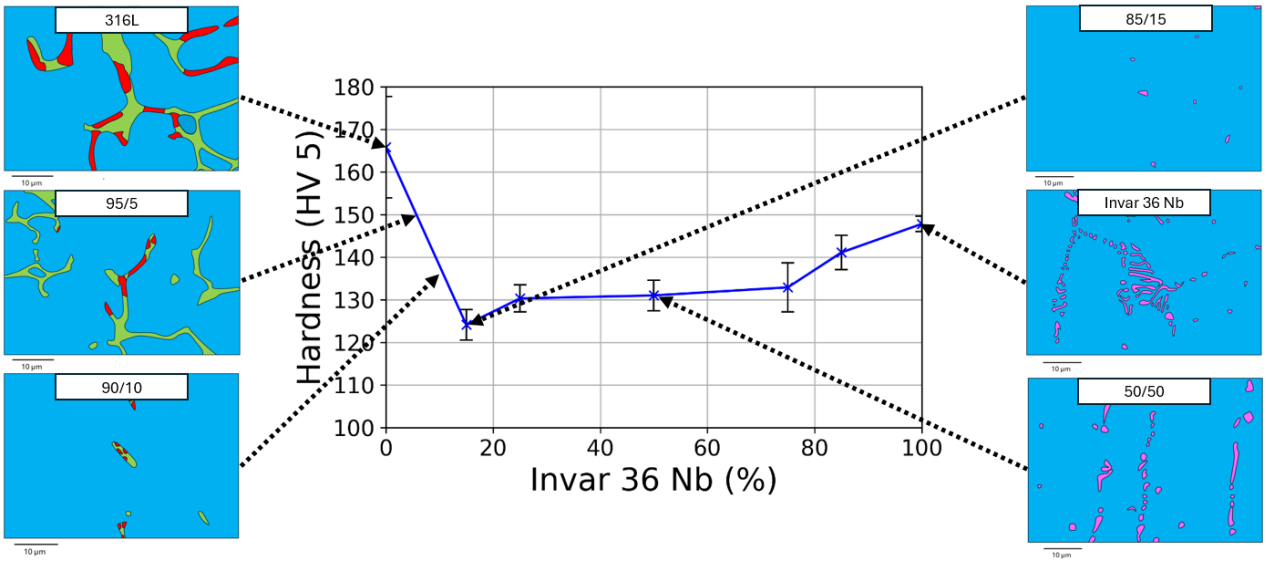

Fig. 4. Hardness and microstructure evolution as a function of the proportion of Invar 36 Nb.

Mechanical Properties

The mechanical properties of the different alloys are then evaluated by tensile testing. Figure 5a shows the evolution of ultimate tensile strength (UTS) and elongation at break (A) as a function of chemical composition. Pure 316L stainless steel achieves a maximum stress of 586 MPa with an elongation at break of approximately 23%. While the UTS obtained is consistent with the values reported in the literature, the elongation at break is lower: Wang et al., for example, report a UTS of 526,9 MPa associated with an elongation of 46% with a WAAM-CMT process [18]. Saboori et al. also indicate that several DED processes lead to superior properties [19]. This reduced ductility can be attributed to the presence of the highly brittle σ phase, as well as to defects generated at the interlayer interfaces.

The addition of 25% Invar 36 Nb significantly alters the mechanical behavior: the UTS decreases while the elongation at break (A) increases sharply, from 23% to 44%. This improvement in ductility is consistent with microhardness observations and can be explained by the disappearance of ferritic and σ phases in the microstructure. When the Invar 36 Nb content reaches 50% or 75%, the UTS increases while the elongation decreases. This change is linked to the gradual increase in the fraction of carbides, which increases mechanical strength by blocking the movement of dislocations but reduce ductility by generating local stress concentrations favorable to crack initiation. However, pure Invar 36 Nb does not follow this reasoning: it has both a lower UTS and a lower elongation than compositions with 50% and 75% Invar 36 Nb. One might expect higher strength due to the high density of carbides. However, these hard particles create significant mechanical heterogeneities that promote premature failure. Ultimately, Invar 36 Nb has a UTS of 450 MPa and an elongation of approximately 29%. These results fall between those obtained by Veiga et al. (464 MPa, 49%) [17] and Jiao et al. (569 MPa, 27%) [20]. A similar trend of decreasing UTS is also observed in the work of Guo et al., although these authors report minimal elongation for intermediate Invar 36 contents (30–40%) [11]. This minimal elongation is not observed in this study.

Thermal Expansion of Alloys

Invar 36 Nb was chosen for its very low coefficient of thermal expansion (CTE), a property that is essential to maintain in the gradient. Indeed, too much variation in CTE between two materials can lead to a significant accumulation of thermal stresses, which can cause premature failure. It is therefore essential to know precisely how CTE changes according to chemical composition to optimize the transition between 316L steel and Invar 36 Nb.

The evolution of the CTE between 25°C and 100°C as a function of chemical composition is shown in Figure 5b. The CTE of 316L steel is $15{,}3\times10^{-6}$ °C^{-1}, which corresponds to the expected values. With the addition of Invar 36 Nb, the CTE initially increases slightly, reaching $17{,}3\times10^{-6}$ °C^{-1} for the alloy with 50% Invar 36 Nb. This increase is attributed to the disappearance of the ferrite and σ phases, whose thermal expansion is lower than that of austenite. Above 50% Invar, the CTE then begins to decrease, but this decrease only becomes significant above 75% Invar, where it falls from $13{,}4\times10^{-6}$ °C^{-1} to only $2{,}4\times10^{-6}$ °C^{-1} for pure Invar 36 Nb. This significant decrease can be explained by spontaneous magnetostriction: below the Curie temperature, the appearance of ferromagnetism causes the crystal lattice to expand, which compensates for thermal contraction [21]. The appearance of this ferromagnetic behavior is not linear with composition, because chromium-rich austenite disrupts magnetic coupling until a critical fraction of Invar 36 Nb is reached. Beyond that point, a coherent magnetic order is established, and the CTE drops sharply. The CTE obtained for pure Invar 36 Nb is lower than that reported by Aldalur et al. for a WAAM-PAW process (4.32×10^{-6} °C^{-1}), but remains slightly higher than their reference value ($2{,}29\times10^{-6}$ °C^{-1}) [22] and those obtained by laser powder bed fusion [23]. The non-linear trend of this evolution is consistent with the observations of Hofmann et al. [9]. On the contrary, Guo et al. report a significant decrease with 50% Invar [11], which is not observed here.

Corrosion Resistance

316L stainless steel was chosen for its low cost and excellent chemical properties, including very good corrosion resistance. This corrosion resistance is therefore studied to validate the use of 316L steel and to characterize the influence of Invar content on chemical behavior. Different parameters can be determined from the intensity curves as a function of potential: the corrosion potential (E_{corr}), the corrosion current (I_{corr}), the pitting potential (E_{pit}), and the pitting current (I_{pit}). The corrosion current I_{corr} characterizes the corrosion rate, but it is very sensitive to the surface condition and experimental conditions. To compare materials with each other, the difference $\Delta E = E_{pit} - E_{corr}$ is therefore preferred. E_{corr} corresponds to the natural potential adopted by the metal in the environment studied, without the application of current, and is an indicator of generalized corrosion resistance. E_{pit} indicates the potential at which localized pitting corrosion begins, i.e., the voltage at which the protective passive film becomes locally unstable. Improved corrosion resistance results in a higher pitting potential. Thus, ΔE represents the potential range in which the material remains passive: the greater ΔE, the higher the corrosion resistance. Figure 5c shows the evolution of ΔE as a function of the proportion of Invar 36 Nb.

For 316L stainless steel, a ΔE of 635 mV is measured, close to the 620 mV reported by Chen et al. using a WAAM-GMAW process [24]. Chen et al. also showed that the presence of the σ phase degrades the corrosion resistance, as it creates areas depleted in chromium [24]. However, for stainless steels, the corrosion resistance is highly dependent on the chromium content, which forms a protective Cr_2O_3 film. Localized corrosion occurs when this oxide film is disturbed [25]. Wang et al. obtained a higher ΔE of 740 mV, as their 316L steel manufactured by WAAM-CMT did not contain any σ phase [26]. Then, as the proportion of Invar 36 Nb increases, the passivation range ΔE decreases. With the addition of 15% Invar 36 Nb, the corrosion resistance remains good because the chromium content is still high enough to have a stable passive film. Beyond the addition of 25% Invar 36 Nb, the chromium content falls below the threshold required for homogeneous passivation, and chromium-depleted areas appear, promoting pitting corrosion. Thus, ΔE is between 406 mV and 322 mV when the chromium content is between 25% and 85%. ΔE continues to decrease for pure Invar

36, which has a ΔE of only 230 mV. This material, therefore, exhibits low corrosion resistance, a result consistent with the literature. This decrease is mainly due to the reduction in chromium content as the proportion of Invar 36 Nb increases, thereby reducing the ability to form the protective Cr_2O_3 film.

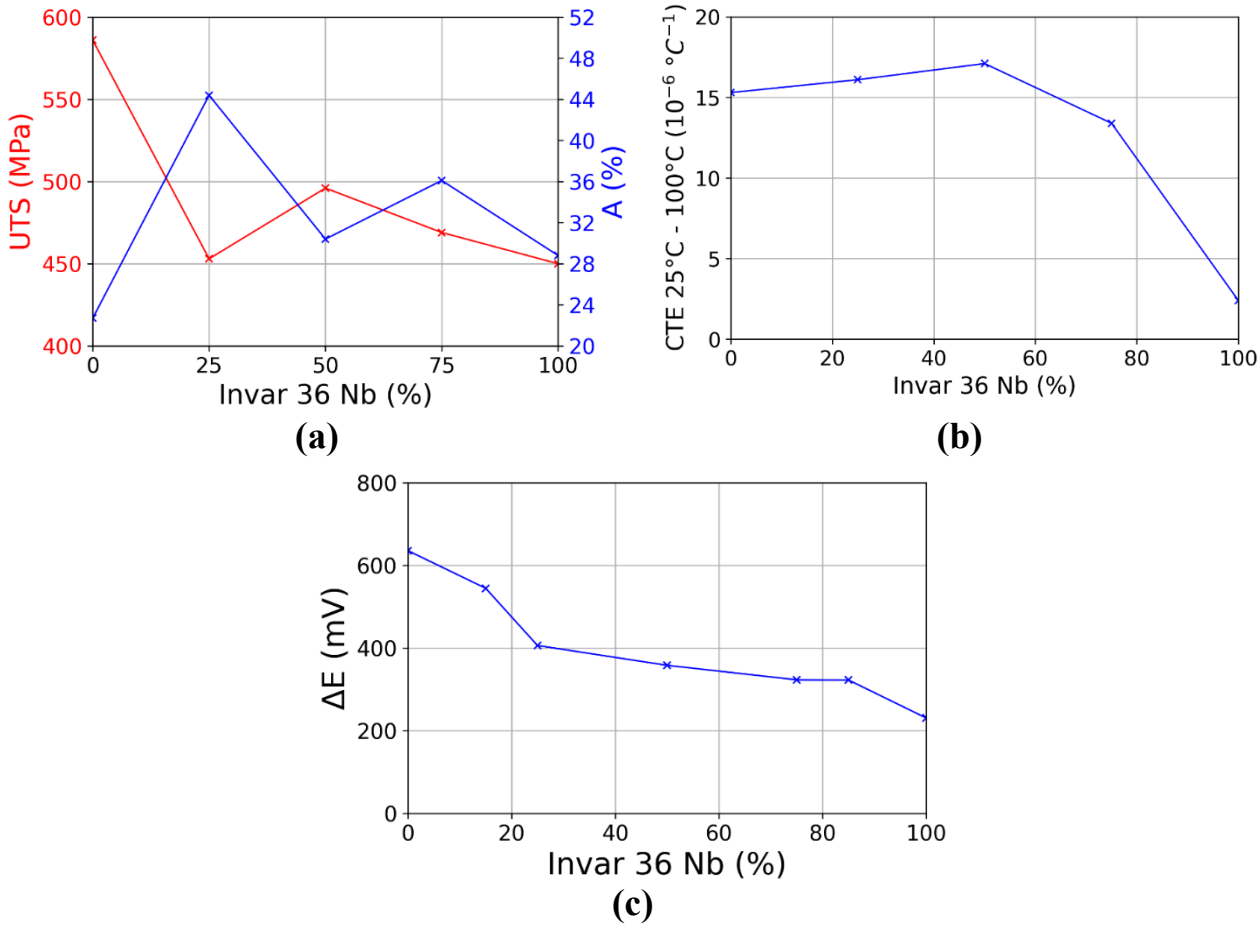

Fig. 5. Evolution of different properties of the multi-material (316L/Invar36Nb) as a function of Invar 36 Nb rate: (a) ultimate tensile strength (UTS) and elongation at break; (b) CTE coefficient; and (c) passivation layer.

4. Conclusion

Optimization of the WAAM-PAW process has enabled the successful production of a series of homogeneous 316L–Invar 36 Nb alloys free of defects. Their characterization (Table 5) highlights several conclusions:

- 316L stainless steel has the highest hardness (166 HV) due to the presence of ferrite and σ phase. The addition of Invar 36 Nb eliminates these phases and leads to the formation of carbides, which lowers the hardness to a minimum of 124 HV for 15% Invar 36 Nb. Beyond that, the hardness gradually increases to 148 HV for pure Invar 36 Nb as the proportion of carbides increases.
- The maximum UTS is obtained for 316L stainless steel (586 MPa). For other compositions, the UTS remains relatively stable between 450 and 496 MPa. The elongation at break is highest for the alloy containing 25% Invar 36 Nb, where the disappearance of the ferrite and σ phases and the low fraction of carbides promote better ductility.
- The coefficient of thermal expansion (CTE) does not follow a linear trend. It remains high between 0% and 75% of Invar 36 Nb, then drops sharply from 13,4 × 10^{-6} $°C^{-1}$ to 2,4 × 10^{-6} $°C^{-1}$ between 75% and 100% of Invar. Indeed, with a high Invar 36 Nb content, the alloy becomes strongly ferromagnetic, and the “Invar” effect becomes clearly apparent.

- Excellent corrosion resistance is observed for Invar 36 Nb contents below 15%, with a passivation range from 635 mV (316L) to 544 mV (15% Invar). Above this level, chromium depletion limits the formation of a stable passive film, which degrades pitting resistance.

These results show that, despite some variations, the mechanical properties of the intermediate alloys remain similar. The UTS is lowest for pure Invar 36 Nb, while the minimum elongation is observed for 316L steel. This means that within a functionally graded material, the intermediate compositions do not constitute an area of mechanical weakness, which is essential for ensuring the structural integrity of the gradient. Then, the CTE is the property that changes the most significantly. To avoid sudden variations in CTE that could generate thermal stresses and cause premature failure, the gradient will need to incorporate much finer composition transitions on the Invar 36 Nb-rich side. Conversely, corrosion resistance is only satisfactory for high 316L stainless steel contents. However, a change in chemical behavior does not lead to immediate mechanical failure. Therefore, it is not necessary to introduce several intermediate steps for this property, and a single composition rich in 316L can be incorporated into the gradient.

This analysis thus provides a rational basis for designing a gradient between 316L and Invar 36 Nb: smooth gradual transition to control thermal expansion, but direct transition for corrosion resistance, two key elements for developing a high-performance, durable gradient.

Table 5. Summary of the properties for the different characterized alloys.

Alloy (316L [%]/Invar [%])	100/0	85/15	75/25	50/50	25/75	15/85	0/100
Microhardness [HV 5]	165,8	124,1	130,3	131,0	132,9	141,1	147,8
UTS [Mpa]	586	/	453	496	469	/	450
A [%]	22,7	/	44,4	30,4	36,1	/	28,8
CTE [10^{-6} °C $^{-1}$]	15,3	/	16,1	17,1	13,4	/	2,4
ΔE [mV]	635,5	544,5	406	358	323	322,5	230,5

References

[1] J. N. DuPont, « Microstructural evolution and high temperature failure of ferritic to austenitic dissimilar welds », *International Materials Reviews*, vol. 57, nº 4, p. 208-234, juill. 2012, doi: 10.1179/1743280412Y.0000000006.

[2] A. Nazir *et al.*, « Multi-material additive manufacturing: A systematic review of design, properties, applications, challenges, and 3D printing of materials and cellular metamaterials », *Materials & Design*, vol. 226, p. 111661, févr. 2023, doi: 10.1016/j.matdes.2023.111661.

[3] A. Shah, R. Aliyev, H. Zeidler, et S. Krinke, « A Review of the Recent Developments and Challenges in Wire Arc Additive Manufacturing (WAAM) Process », *JMMP*, vol. 7, nº 3, p. 97, mai 2023, doi: 10.3390/jmmp7030097.

[4] T. A. Rodrigues *et al.*, « Wire and arc additive manufacturing of 316L stainless steel/Inconel 625 functionally graded material: development and characterization », *Journal of Materials Research and Technology*, vol. 21, p. 237-251, nov. 2022, doi: 10.1016/j.jmrt.2022.08.169.

[5] X. Chen *et al.*, « A functionally graded material from TC4 to 316L stainless steel fabricated by double-wire + arc additive manufacturing », *Materials Letters*, vol. 300, p. 130141, oct. 2021, doi: 10.1016/j.matlet.2021.130141.

[6] W. S. Park, M. S. Chun, M. S. Han, M. H. Kim, et J. M. Lee, « Comparative study on mechanical behavior of low temperature application materials for ships and offshore structures: Part I—Experimental investigations », *Materials Science and Engineering: A*, vol. 528, nº 18, p. 5790-5803, juill. 2011, doi: 10.1016/j.msea.2011.04.032.

[7] M. Teshigawara, M. Harada, M. Ooi, T. Kai, F. Maekawa, et M. Futakawa, « Development of invar joint for hydrogen transfer line in JSNS », *Journal of Nuclear Materials*, vol. 431, nº 1-3, p. 212-217, déc. 2012, doi: 10.1016/j.jnucmat.2011.11.031.

[8] A. Cornelius, L. Jacobs, M. Lamsey, L. McNeil, W. Hamel, et T. Schmitz, « Hybrid manufacturing of Invar mold for carbon fiber layup using structured light scanning », *Manufacturing Letters*, vol. 33, p. 133-142, sept. 2022, doi: 10.1016/j.mfglet.2022.07.019.

[9] D. C. Hofmann *et al.*, « Developing Gradient Metal Alloys through Radial Deposition Additive Manufacturing », *Sci Rep*, vol. 4, nº 1, p. 5357, juin 2014, doi: 10.1038/srep05357.

[10] A. Arbogast, S. Roy, A. Nycz, M. W. Noakes, C. Masuo, et S. S. Babu, « Investigating the Linear Thermal Expansion of Additively Manufactured Multi-Material Joining between Invar and Steel », *Materials*, vol. 13, nº 24, p. 5683, déc. 2020, doi: 10.3390/ma13245683.

[11] H. Guo, D. Liu, M. Xu, Z. Dong, et L. Zhang, « Preparation, characterization and composition optimization design of laser powder bed fusion continuously graded Invar36/316L stainless steel alloys », *Materials Characterization*, vol. 209, p. 113709, mars 2024, doi: 10.1016/j.matchar.2024.113709.

[12] T. Osuki, K. Ogawa, et H. Hirata, « Analysis of the solidification process in Fe–36%Ni weld metal with NbC crystallization », *Welding International*, vol. 20, nº 2, p. 116-126, févr. 2006, doi: 10.1533/wint.2006.3544.

[13] D. Jafari, T. H. J. Vaneker, et I. Gibson, « Wire and arc additive manufacturing: Opportunities and challenges to control the quality and accuracy of manufactured parts », *Materials & Design*, vol. 202, p. 109471, avr. 2021, doi: 10.1016/j.matdes.2021.109471.

[14] X. Yu *et al.*, « Effect of composition gradient design on microstructure and mechanical properties of dual-wire plasma arc additively manufactured 316L/IN625 functionally graded materials », *Materials Chemistry and Physics*, vol. 307, p. 128121, oct. 2023, doi: 10.1016/j.matchemphys.2023.128121.

[15] U. Gürol, E. Kocaman, S. Dilibal, et M. Koçak, « A comparative study on the microstructure, mechanical properties, wear and corrosion behaviors of SS 316 austenitic stainless steels manufactured by casting and WAAM technologies », *CIRP Journal of Manufacturing Science and Technology*, vol. 47, p. 215-227, déc. 2023, doi: 10.1016/j.cirpj.2023.10.005.

[16] A. Iturrioz, E. Ukar, et J. C. Pereira, « Influence of the manufacturing strategy on the microstructure and mechanical properties of Invar 36 alloy parts manufactured by CMT-WAAM », *Int J Adv Manuf Technol*, déc. 2024, doi: 10.1007/s00170-024-14853-5.

[17] F. Veiga, A. Suárez, T. Artaza, et E. Aldalur, « Effect of the Heat Input on Wire-Arc Additive Manufacturing of Invar 36 Alloy: Microstructure and Mechanical Properties », *Weld World*, vol. 66, nº 6, p. 1081-1091, juin 2022, doi: 10.1007/s40194-022-01295-4.

[18] C. Wang, T. G. Liu, P. Zhu, Y. H. Lu, et T. Shoji, « Study on microstructure and tensile properties of 316L stainless steel fabricated by CMT wire and arc additive manufacturing », *Materials Science and Engineering: A*, vol. 796, p. 140006, oct. 2020, doi: 10.1016/j.msea.2020.140006.

[19] A. Saboori, A. Aversa, G. Marchese, S. Biamino, M. Lombardi, et P. Fino, « Microstructure and Mechanical Properties of AISI 316L Produced by Directed Energy Deposition-Based Additive Manufacturing: A Review », *Applied Sciences*, vol. 10, nº 9, p. 3310, mai 2020, doi: 10.3390/app10093310.

[20] G. Jiao *et al.*, « High performance ultrasonic vibration assisted Wire-arc directed energy deposition of Invar alloy », *Journal of Materials Processing Technology*, vol. 332, p. 118534, nov. 2024, doi: 10.1016/j.jmatprotec.2024.118534.

[21] T. Wegener *et al.*, « On the structural integrity of Fe-36Ni Invar alloy processed by selective laser melting », *Additive Manufacturing*, vol. 37, p. 101603, janv. 2021, doi: 10.1016/j.addma.2020.101603.

[22] E. Aldalur, A. Suárez, et F. Veiga, « Thermal expansion behaviour of Invar 36 alloy parts fabricated by wire-arc additive manufacturing », *Journal of Materials Research and Technology*, vol. 19, p. 3634-3645, juill. 2022, doi: 10.1016/j.jmrt.2022.06.114.

[23] G. Huang, G. He, Y. Liu, et K. Huang, « Anisotropy of microstructure, mechanical properties and thermal expansion in Invar 36 alloy fabricated via laser powder bed fusion », *Additive Manufacturing*, vol. 82, p. 104025, févr. 2024, doi: 10.1016/j.addma.2024.104025.

[24] X. Chen, J. Li, X. Cheng, H. Wang, et Z. Huang, « Effect of heat treatment on microstructure, mechanical and corrosion properties of austenitic stainless steel 316L using arc additive manufacturing », *Materials Science and Engineering: A*, vol. 715, p. 307-314, févr. 2018, doi: 10.1016/j.msea.2017.10.002.

[25] C. Penot, « Corrosion performance of an austenitic stainless steel fabricated by wire arc additive manufacturing ».

[26] C. Wang, P. Zhu, F. Wang, Y. H. Lu, et T. Shoji, « Anisotropy of microstructure and corrosion resistance of 316L stainless steel fabricated by wire and arc additive manufacturing », *Corrosion Science*, vol. 206, p. 110549, sept. 2022, doi: 10.1016/j.corsci.2022.110549.